Relationship between corotating vortex-pair equilibria and a single vortex in an external deformation field

Uwe Ehrenstein[a)]
*Laboratoire J.-A. Dieudonné, Université de Nice - Sophia Antipolis, Parc Valrose, F-06108 Nice Cedex 02,
France*

Stéphane Le Dizès
*Institut de Recherche sur les Phénomènes Hors Équilibre, UMR 6594 CNRS/Universités Aix-Marseille,
49 rue F. Joliot-Curie, Boite Postale 146, F-13384 Marseille Cedex 13, France*

Two-dimensional corotating vortex pairs are computed as equilibrium solutions of the Euler equations and the influence of one vortex on the other is characterized in terms of a deformation field acting on an isolated vortex region. It is shown, by computing equilibrium states for a single vortex within an equivalent strain field, that the external rotating strain accounts for the elliptic deformation of the streamlines near the center of each vortex. Critical states, as a function of the strain rate, are reached when stagnation points start to penetrate the vortex regions at the outer boundary. While critical states for a single vortex within a uniform external rotating strain field consist of elliptical corner solutions, the vortex shapes lose the elliptical symmetry in the corotating case. We show that these asymmetric equilibrium states can be captured by a single vortex model if we consider higher order terms in the deformation field. We also demonstrate that the critical strain rates are of the same order of magnitude for both the single-vortex model and the interacting vortex pair. © *2005 American Institute of Physics*. [DOI: 10.1063/1.1949192]

I. INTRODUCTION

Coherent vortices are ubiquitous of most high Reynolds number flows. In shear flows, such as wakes, jets, or mixing layers, they can be formed by a two-dimensional Kelvin-Helmholtz instability. The resulting two-dimensional vortices are then subject to complex dynamical behaviors including vortex pairing and/or three-dimensional instabilities, which often lead to a transition to a disordered state. These complex evolutions are also present in simpler systems, such as the one composed of two identical corotating vortices. Corotating vortices are indeed known to be subject to a three-dimensional instability (the elliptical instability) and to merge if they are sufficiently close. In the present work, our goal is to demonstrate that both merging conditions and elliptical instability characteristics for corotating vortices can be captured by considering a simple model based on a single vortex in a straining field.

The elliptical instability is a generic phenomenon affecting two-dimensional strained vortices. It has been evidenced in systems as different as vortex rings, vortex pairs, wakes, shear layers, and elliptic cylinders (see Ref. 1 for a review). The growth rate of this instability is proportional to the local strain rate in the vortex center.[1] However, this strain rate results from a complicated interaction process between the vortex and a background external straining field induced by other vortices.[2,3] Recently, Le Dizès and Verga[4] demonstrated that the elliptic deformation of the vortex cores in a two-corotating-vortices system was well predicted by the

simple model of a vortex in a weak rotating strain field. Here, similar results are shown, but they are not limited to distant vortices or weak strain field interactions. Our numerical method allows a comprehensive comparison of corotating vortex solutions with the solution of a vortex in a rotating strain field up to the parameters for which the equilibrium solutions disappear.

The disappearence of the equilibrium solution is a two-dimensional phenomenon occuring in both systems. In most available studies, this phenomenon has been analyzed in a purely inviscid framework for idealized vortices with vorticity located in finite regions. Moore and Saffman[5] computed the strain rate above which a strained elliptical vortex region with constant vorticity becomes unstable. Kida[6] extended their analysis to account for shear and rotating strain fields. Later, more sophisticated numerical methods based on contour dynamics were used to consider nonuniform vorticity distributions and to analyze the temporal evolution above threshold.[7,8] Similar studies were performed for corotating vortex pairs. For this configuration, it has soon been evidenced that the two corotating vortices merge into a single one when the distance between their center is smaller than a certain distance. A critical separation distance was first evaluated by Saffman and Szeto[9] by using inviscid uniform vortices. Subsequently, models for two-dimensional vortex merging based on contour dynamics have been proposed[10] and high-resolution simulation of vortex merger has been performed,[11] to cite a few. It is only recently that an effort has been made to compare the experimental data[12,13] of the stage just prior merging with the equilibrium states obtained in the inviscid framework near threshold.[14] In Ref. 14, it has been argued that the critical separation distance could be

---

[a)]Author to whom correspondence should be addressed. Electronic mail:
uwe.ehrenstein@unice.fr

associated with the onset of vortex merging. In the present work, we go one step further by trying to connect this onset with the critical parameter of a single vortex in a straining field.

As in Ref. 14, our approach uses the numerical tool which has been developed by Ehrenstein and Rossi.[15] This numerical code is able to compute equilibrium solutions of the two-dimensional Euler equations composed of finite regions of nonuniform vorticity. It can be used to determine corotating vortex solutions as well as the solution of a single vortex in an external strain field. It is therefore well adapted to the aim of the present investigation which is to compare the equilibrium states of both systems.

The paper is organized as follows. In Sec. II the procedure capable of computing nonlinear Euler equilibria is briefly outlined. In Sec. III the deformation field exerted from one vortex on the other in the corotating case is characterized. The question of critical states is addressed in Sec. IV. A single vortex within a rotating strain as well as the two-corotating-vortices system is considered, and a model of a single vortex within a higher deformation field is proposed. Some conclusions are drawn in Sec. V.

II. NONLINEAR EULER SOLUTION MODEL AND SOLUTION PROCEDURE

In previous works,[14,15] the numerical procedure used by Saffman and Szeto[9] has been generalized to compute nonlinear Euler solutions for a corotating vortex pair with nonuniform vorticity distributions. The approach, which is briefly outlined in the following (details may be found in Ref. 15), is based on the computation of the deformation of the streamlines, by considering Green's function integrals. In the absence of any external strain field, the undisturbed circular vortex with area S is parametrized by the radial position $r_0(\omega)$ which is a function of vorticity. In the perturbed case, the vorticity contours lie on lines such that

$$r(\omega, \theta)^2 = r_0(\omega)^2 + f(\omega, \theta), \quad 0 \leq \theta \leq 2\pi \tag{1}$$

(for the unknown deformation $f(\omega, \theta)$ to be determined) and the Green's function integrals over the perturbed vortex area S are expressed as vorticity integrals

$$\psi(x,y) = -\frac{1}{4\pi} \int_{\omega_{min}}^{\omega_{max}} \int_0^{2\pi} \log\{[x - x(\omega', \theta')]^2$$

$$+ [y - y(\omega', \theta')]^2\} \frac{1}{2}\omega'\left(-\frac{\partial r^2}{\partial \omega}(\omega', \theta')\right)d\omega' \, d\theta'. \tag{2}$$

The vorticity inside the vortex varies from the maximum value ω_{max} at the center $r=0$ [that is, $f(\omega_{max}, \theta)=0$] to the minimum value ω_{min} at the outer vorticity contour.

For the configuration of two equal corotating vortices with the distance L between the vortex centers, the total streamfunction inside the vorticity region 1 reads

$$\psi_t(x,y) = \psi(x,y) + \psi_e(x,y), \tag{3}$$

in the coordinate system (x,y) with origin O the center of vortex 1. The streamfunction $\psi(x,y)$ is given by the vorticity
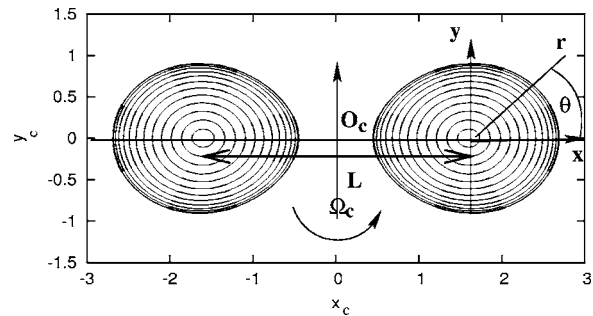

FIG. 1. Streamlines, in the rotating reference frame (x_c, y_c), for the equilibrium state of two parabolic corotating vortices with a distance $L=3.2$ between the vortex centers.

integral (2) and the external streamfunction $\psi_e(x, y)$ decomposes into

$$\psi_e(x,y) = \psi_2(x + L, y) + \frac{1}{2}\Omega_c[(x + L/2)^2 + y^2]. \tag{4}$$

The streamfunction $\psi_2(x+L, y)$ (again defined as a vorticity integral over vortex region 2) corresponds to the contribution of vortex 2 at a distance L and the whole vortex system is rotating around the center O_c at the angular frequency Ω_c. An equilibrium state for the configuration of two equal corotating vortices with a sketch of the coordinate system is represented in Fig. 1. The corresponding steady solutions of the Euler equations satisfy the constraint that isovorticity contours are streamlines, the coordinates in both the vortex regions being expressed in terms of the perturbed radius (1), and are hence a function of (ω, θ). Using Chebyshev collocation in ω and Fourier collocation in θ, the deformations of the streamlines $f(\omega, \theta)$ in both vorticity regions may be computed solving numerically a nonlinear system (cf. Refs. 14 and 15), the continuation parameter being the (decreasing) distance L. The vortex centers are stagnation points in the rotating frame of reference which provides the extra condition to determine the rotation rate Ω_c. The equilibrium configurations are supposed to be symmetric with respect to the x axis. In the present work each vortex has been discretized using up to 18 Chebyshev-collocation points in ω and 82 Fourier-collocation points for the whole contour in θ.

When the corotating vortices are far apart from each other the isovorticity contours (or equivalently the streamlines) are approximately circular. Hence, for large distances L between the vortex centers the computations start with initial axisymmetric vorticity distributions. In the present investigation an initial parabolic vorticity distribution

$$\omega(r) = \omega_{max}(1 - r^2), \quad 0 \leq r \leq 1, \tag{5}$$

as well as a Gaussian profile

$$\omega(r) = \omega_{max} \exp(-r^2), \quad 0 \leq r \leq 1 \tag{6}$$

have been considered. The maximum of vorticity at the center is $\omega_{max}=2$ [respectively, $\omega_{max}=1/(1-e^{-1})$] for the parabolic distribution (respectively, the Gaussian profile) for the circulation to be π (which is held constant throughout the continuation procedure). The equilibrium state in Fig. 1 has been computed starting with the initial parabolic profile.

III. DEFORMATION FIELD IN THE COROTATING VORTICES SYSTEM

It may easily be checked deriving the Green's function that the Taylor expansion of $\psi_e(x,y)$ in (3) at the center of vortex 1 writes up to third order:

$$\psi_e(x,y) \sim v\,x + \tfrac{1}{2}[(\hat{\Omega}_e + \hat{\gamma}_e)x^2 + (\hat{\Omega}_e - \hat{\gamma}_e)y^2]$$
$$+ \tfrac{1}{6}\hat{\eta}_e(3xy^2 - x^3). \tag{7}$$

The odd derivatives in y are zero, the vortex shape being symmetric with respect to the x axis. The first-order term $v\,x$ in (7) is zero as long as the vortex shape is symmetric with respect to the y axis, for instance, as long as the isolines of vorticity are elliptic. However, the isolines of vorticity deform asymmetrically for decreasing distances between the vortex centers (cf. Fig. 1). The vortex centers being stagnation points for the model, v is determined throughout the solution procedure via the condition

$$v = -\frac{\partial \psi}{\partial x}(0,0). \tag{8}$$

The second-order terms in (7) account for the rotating strain that vortex 2 exerts on vortex 1 with

$$\hat{\gamma}_e = \frac{\partial^2 \psi_2}{\partial x^2}(L,0) = -\frac{\partial^2 \psi_2}{\partial y^2}(L,0), \quad \hat{\Omega}_e = \Omega_c. \tag{9}$$

The third-order terms (which are nonzero for asymmetric, with respect to the y axis, vortex deformations) are

$$\hat{\eta}_e = \frac{\partial^3 \psi_2}{\partial x\,\partial y^2}(L,0) = -\frac{\partial^3 \psi_2}{\partial x^3}(L,0). \tag{10}$$

Asymptotic external strain values and rotation rates may be recovered when the streamlines are approximately circular (which supposes large distance values L). For this asymptotic case $v=0$ in (7) and the influence of one vortex on the other is then equivalent to that of a point vortex with same circulation Γ. The condition for the vortex center to be a stagnation point becomes

$$-\frac{\Gamma}{2\pi L} + \frac{\Omega_c L}{2} = 0. \tag{11}$$

The asymptotic strain imposed by vortex 2 on vortex 1 is

$$\hat{\gamma}_e = \frac{\Gamma}{2\pi L^2} \tag{12}$$

and the asymptotic higher order term in (10) is

$$\hat{\eta}_e = \frac{\Gamma}{\pi L^3}. \tag{13}$$

Hence for a given strain, the following asymptotic relationships hold:

$$\hat{\Omega}_e = \Omega_c = 2\hat{\gamma}_e, \quad \hat{\eta}_e = \sqrt{\frac{\pi}{\Gamma}}(2\hat{\gamma}_e)^{3/2}. \tag{14}$$

The strain value $\hat{\gamma}_e$ in (9) is compared with the asymptotic expression (12) in Fig. 2, as a function of the distance L, for the initial parabolic vorticity distribution (5).
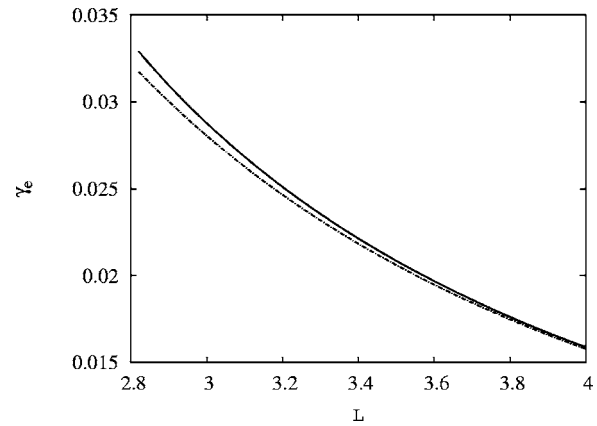

FIG. 2. Strain rate γ_e acting on vortex 1 in the corotating vortices configuration, as a function of the distance between the vortex centers L;——: computed value for an initial parabolic vorticity distribution. -.-: asymptotic value [expression (12)].

The normalized strain rate $\gamma_e = \hat{\gamma}_e/\omega_{\max}$ is shown for values of L varying from 4 to 2.85 and a good agreement is observed. The critical value $L_c=2.85$ is the smallest value for which the equilibrium state of corotating vortices exists for the initial parabolic state considered here (critical vortex configurations are addressed in Sec. IV).

The relationships (14) provide the asymptotic values of the rotation rate $\hat{\Omega}_e = \Omega_c$ as well as the higher order term $\hat{\eta}_e$, as a function of $\hat{\gamma}_e$. These quantities are compared in Fig. 3 with the value (10) and the rotation rate $\Omega_c = \hat{\Omega}_e$ as provided by the numerical solution procedure. The results are shown as function of γ_e (again all quantities are normalized with respect to $\omega_{\max}$) and it may be seen that the curves almost superimpose. Again, the distance L has been varied from $L=4$ to the critical value $L \approx 2.85$ with the corresponding strain rates shown in Fig. 2.

Figure 1 depicts typical isovorticity contours for equilibrium states and the innermost streamlines inside the vortex regions are seen to be approximately elliptical. The stream-
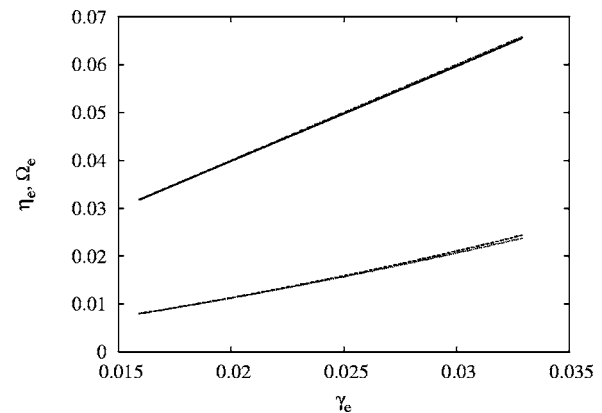

FIG. 3. Characteristics of the equilibrium state of two parabolic corotating vortices from $L=4$ to the critical distance $L \approx 2.85$. Computed (solid line) and asymptotic (dash-dotted line) angular velocity $\Omega_e = \hat{\Omega}_e/\omega_{\max}$; computed (dashed line) and asymptotic (dotted line) higher order deformation rate $\eta_e = \hat{\eta}_e/\omega_{\max}$.
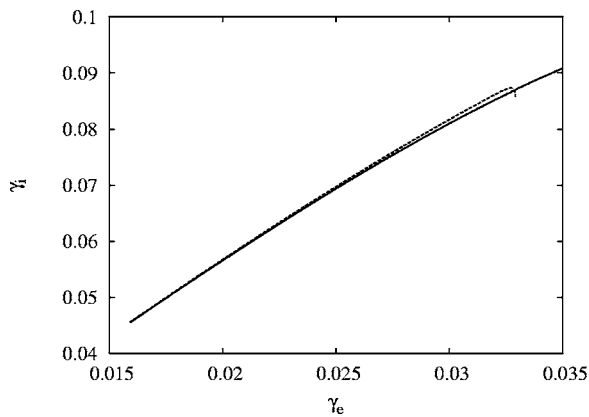
FIG. 4. Internal strain rate γ_i as function of the external strain rate γ_e for two corotating vortices (dashed line) and a single vortex in an external rotating strain field with $\Omega_e = 2\gamma_e$ (solid line). Initial parabolic vorticity distribution in each case.

lines in the vicinity of the vortex centers may be parametrized considering an inner angular velocity $\hat{\Omega}_i$ and an inner strain rate $\hat{\gamma}_i$ such that

$$(\hat{\Omega}_i - \hat{\gamma}_i)x^2 + (\hat{\Omega}_i + \hat{\gamma}_i)y^2 = \epsilon \ll 1. \tag{15}$$

The angular velocity is computed as a by-product of the solution procedure with

$$\hat{\Omega} = -\frac{1}{r}\frac{\partial \psi_t}{\partial r}(\mathbf{r}) = \frac{\partial \psi_t}{\partial \omega}\frac{2}{\partial r^2/\partial \omega}(\omega,\theta) \tag{16}$$

and hence

$$\hat{\Omega}_i = -\lim_{\omega \to \omega_{\max}} \frac{\partial \psi_t}{\partial \omega}\frac{2}{\partial r^2/\partial \omega}(\omega,\theta). \tag{17}$$

The internal strain value γ_i, which is the key parameter for elliptical instability,[1] may then be computed, by determining the minor and major semiaxes of the nearly elliptical most inner streamlines, with respect to the discretization.

The external rotating strain accounts for the elliptical deformation and it is tempting to consider a single vortex within an equivalent external field, that is, the specific case of a single vortex in a rotating strain

$$\psi_e(x,y) = \tfrac{1}{2}[(\hat{\Omega}_e + \hat{\gamma}_e)x^2 + (\hat{\Omega}_e - \hat{\gamma}_e)y^2]. \tag{18}$$

The streamlines of a single vortex within the field (18) deform elliptically and may be computed adapting the solution procedure for the corotating vortices configuration. Considering the asymptotic relationship $\hat{\Omega}_e = 2\hat{\gamma}_e$, a single vortex in the leading-order external rotating strain (18) has been considered for increasing strain rates $\hat{\gamma}_e$. The normalized inner strain $\gamma_i = \hat{\gamma}_i/\omega_{\max}$ for the single-vortex model is compared in Fig. 4 with the results obtained for two corotating vortices, starting with an initial parabolic vorticity distribution. The curves almost superimpose up to the value $\gamma_e \approx 0.033$, which corresponds to the critical distance $L = 2.85$ for the corotating vortices. A similar agreement was also observed by Le Dizès and Verga[4] for two viscous corotating vortices for small values of γ_e. They showed that the inner strain rate in one of the vortices agrees with the asymptotic predictions obtained for

a single vortex in a weak external rotating strain field.[3] Here, by considering nonlinear equilibrium solutions, we have demonstrated that the agreement between both systems concerning the inner strain rate is also good for large deformation fields. The external strain γ_e of the single-vortex configuration can be increased furthermore, up to a limiting value (not shown in Fig. 4) which will be discussed in the following section.

IV. CRITICAL EQUILIBRIUM STATES

At leading order, the influence of one vortex on the other in the corotating case may be interpreted in terms of an external rotating strain. When increasing the strain parameter, limiting equilibrium states will be reached and the question arises whether the analogy between the corotating vortex configuration and that of a single vortex in an external deformation field holds up to critical parameter values.

A. A single vortex within a rotating strain field

In the literature, most works have considered the cases of a pure strain field ($\Omega_e = 0$) and of a shear ($\Omega_e = \gamma_e$) in (18). In both cases, a similar scenario has been observed: When the strain parameter γ_e is increased, the shape of the equilibrium solution becomes more and more deformed, up to a configuration in which a stagnation point (in the rotating reference frame) appears at the outermost contour of the vortex. Above this critical strain value, no equilibrium solution exists: The stagnation point penetrates into the vortex and an erosion process, which carries away the vorticity in the most external layer of the vortex, starts. As demonstrated in Refs. 8 and 16, for instance, the complex dynamical behavior associated with this erosion or stripping process can be captured in an inviscid framework if one uses an adequate "contour surgery" procedure.

The appearance of stagnation points in the vortex boundary for critical strain values is easily identified in our numerical calculation. At the stagnation points, $-\partial r^2/\partial \omega \to \infty$ [cf. Eq. (16)] and the coordinate transformation (1) becomes singular. One may conclude that starting with an initial axisymmetric vorticity distribution and increasing continuously the strain parameter, the limit of the continuation procedure, that is, the limit of the stationary Euler's solution model, is reached whenever a corner is forming.

The critical strain parameter γ_e depends on the vortex profile and on Ω_e. The critical curve in the (γ_e, Ω_e) plane is shown in Fig. 5 for the parabolic profile. Again quantities normalized with respect to the maximum of vorticity $\omega_{\max}$ at the center have been used. The plot of Fig. 5 has been numerically computed, for successive Ω_e, by continuation with respect to γ_e up to the limiting singular solution. The star on the curve corresponds, for instance, to the critical strain value $\gamma_{e_c} = 0.59$ for the shear case ($\Omega_e = \gamma_e$). The corresponding corner solution for this critical shear configuration is shown in Fig. 6.

A Gaussian vortex (6) in an external shear ($\Omega_e = \gamma_e$) has been considered by Mariotti *et al.*,[16] who report the critical strain value $\gamma_{e_c} = 0.067$ above which breakup of the vortex occurs. Considering the initial Gaussian profile (6), the criti-
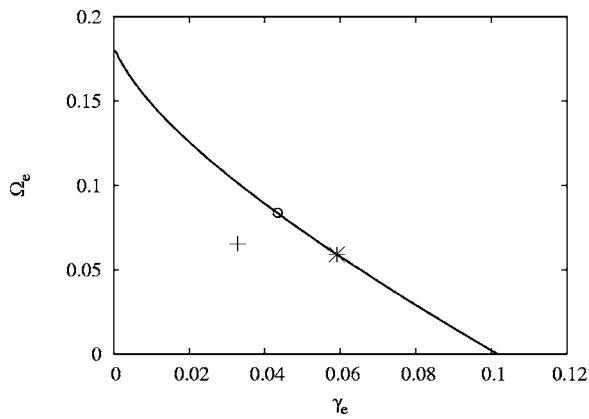
FIG. 5. Critical parameter values (γ_e, Ω_e) for a parabolic vortex in a rotating strain field. $*$, pure shear case $(\gamma_e = \Omega_e)$; $\bigcirc$, corotating vortex case $(\gamma_e = \Omega_e/2)$. The critical strain rate for the two-corotating-vortices is indicated by a cross $(+)$.

FIG. 7. Minimum angular velocity Ω_o for a vortex in a pure shear $(\gamma_e = \Omega_e)$ as a function of the strain rate γ_e. ——, parabolic vorticity distribution; …, Gaussian-like vortex.

cal state where the corners are forming occurs at $\gamma_{e_c} = 0.064$ for the present Euler's solution model which compares favorably with the results in Ref. 16. For both the initial parabolic vorticity distribution and the Gaussian vortex family, the angular frequency (16) has been computed at the outermost boundary of the vortex and the minimum value $\Omega_o = \hat{\Omega}(\omega_{\min}, 0)/\omega_{\max}$ is found at $\theta = 0$ (the corners appear at the points of intersection between the outermost boundary of the vortex and the x axis). The result is shown in Fig. 7 for increasing γ_e, for the shear case $(\gamma_e = \Omega_e)$, for the minimum angular frequency Ω_o tending to zero at the critical strain values. The difference between both curves is that for the Gaussian profile the curve exhibits a limit point in the continuation parameter and then γ_e slightly decreases for vanishing Ω_o. The initial Gaussian distribution exhibits a nonzero cutoff value of vorticity at the boundary, in contrast to the parabolic profile. There is some evidence that limit points in the continuation parameter appear generically when non-
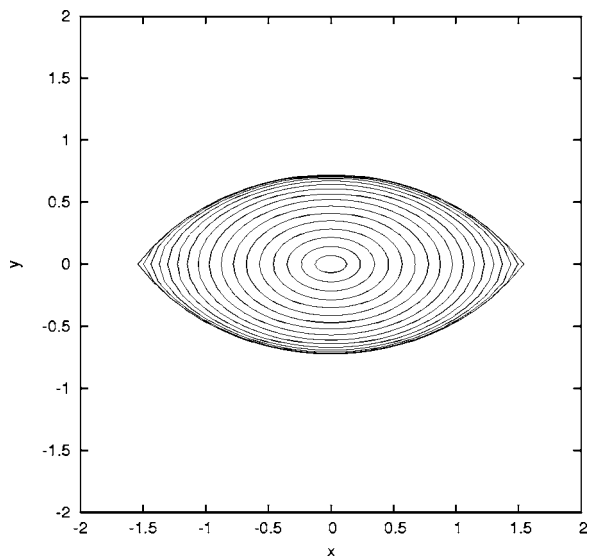
zero cutoff values in the vorticity distribution are considered, as demonstrated, for instance, in Ref. 14 for the corotating vortices case.

B. Critical states for corotating vortices and higher order deformation field

The critical configuration of two corotating vortices is also obtained when a stagnation point reaches the outer boundary of the vortex. As the center point O_c depicted in Fig. 1 is always the closest stagnation point, the critical configuration is expected to occur when both vortices touch the center point, that is, when the gap δ between both vortices goes to zero. This is the very limit for solutions computed as equilibrium states of the Euler system, using the continuation procedure by decreasing the distance L between the vortex centers. It is worth mentioning that this limit is associated with our numerical procedure which requires the existence of two distinct vortices. Recently, Cerretelli and Williamson[17] have shown for uniform vortices that if this constraint is dropped, the continuation procedure could be pursued. They were, in particular, able to compute a new family of equilibrium states, with a dumb-bell shape. The two-dimensional stability of such dumb-bell solutions remains an open issue.

In Ref. 14 the stability threshold was associated with vanishing of an eigenvalue of the Jacobian matrix, which occurs at a finite gap whenever a vorticity distribution with finite cutoff value is considered. For the parabolic profile with zero vorticity at the vortex boundaries, however, the stability threshold is reached for $\delta = 0$. Hence, in order to avoid the singular solution $\delta = 0$ in the iteration procedure used to locate the zero eigenvalue of the Jacobian matrix, a slightly different initial vorticity distribution with $\omega(r) = \omega_{\max}(1 - 0.99r^2)$, $0 \leqslant r \leqslant 1$, has been considered for the limit point to occur for vanishing δ rather than for $\delta = 0$. The streamlines associated with this limit configuration are shown in Fig. 8. The vorticity distribution along the x_c axis is shown as well. The dotted lines correspond to the state depicted in Fig. 1 whereas the solid line is the vorticity distribution at the limit point.

A single vortex within an external rotating strain field

FIG. 6. Streamlines in the rotating reference frame for the critical equilibrium state of a parabolic vortex in a pure shear $(\gamma_e = \Omega_e \approx 0.059)$.
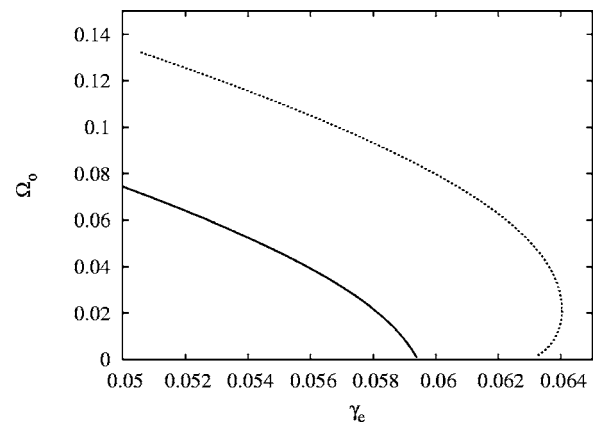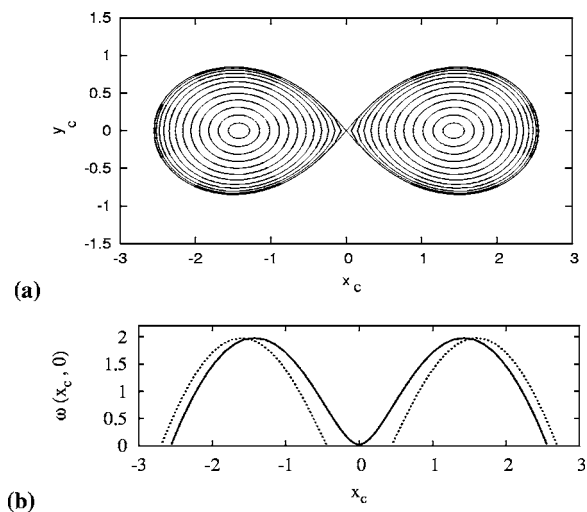
(a)

(b)

FIG. 8. (a) Streamlines in the rotating reference frame for the critical equilibrium state of two parabolic corotating vortices ($L \approx 2.85$; $\gamma_e \approx 0.33$). (b) Vorticity distribution along the $O_c x_c$ direction. ——, critical configuration ($L \approx 2.85$). $\cdots$, configuration shown in Fig. 1 ($L = 3.2$).

FIG. 10. Streamlines for the critical equilibrium state of a single parabolic vortex in a higher order deformation field.

(18) deforms elliptically. In the corotating vortex configurations, however, asymmetric deformations of the streamlines occur when approaching the critical states: indeed, as mentioned above, the corners are forming at the side of the outer vortex boundary which faces the interacting second vortex (cf. Fig. 8). In order to seek for some analogy between a single vortex in an external deformation field and a corotating vortex pair up to critical deformation parameters, higher order terms must certainly be taken into account by considering the deformation field up to third order (7), with the asymptotic relations (14) between the parameters. A convenient quantity in order to characterize the topology of the streamlines is the minimum angular frequency Ω_o, on the outer boundary of the vortex (with Ω_o tending to zero when approaching the singular limiting state). For the parabolic vorticity distribution, this quantity has been computed in the corotating vortices case as a function of γ_e, during the continuation procedure, decreasing L. The result is shown in Fig. 9 as the dashed line. Concerning the single-vortex model,

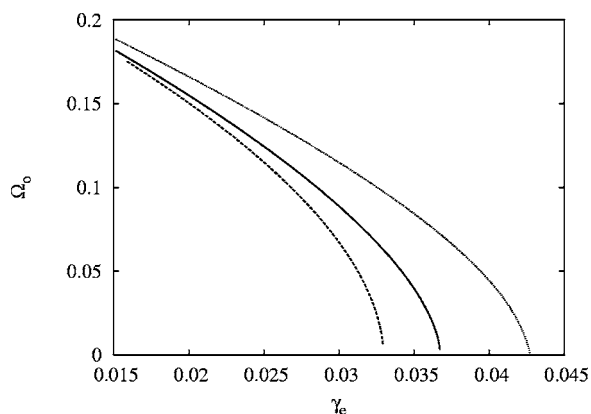first an external rotating strain (18) satisfying $\Omega_e = 2\gamma_e$ has been considered for increasing γ_e. The limit value in γ_e is about 30% higher than the limiting strain in the corotating case. [One may also compare the limiting parameter values for both the corotating case and the single-vortex configuration in the (γ_e, Ω_e) plane depicted in Fig. 5.]

By taking into account the higher order terms in (7), the critical strain parameter is now $\gamma_e \approx 0.37$ which compares much more favorably with the critical strain parameter $\gamma_e \approx 0.33$ for the corotating vortices. The limiting equilibrium state of the single vortex within the higher order deformation field is shown in Fig. 10: now, as expected, the streamlines are asymmetric and a corner is forming at $\theta = \pi$. The topology of the streamlines exhibits the same features as each of the two corotating vortices shown in Fig. 8.

V. CONCLUSION

Isolated vortices within an external deformation field as well as corotating vortices have been computed as equilibrium states of the Euler equations. In the single-vortex case, the external field has been characterized in terms of a strain parameter γ_e whereas for the corotating case the distance between the vortex centers L is the continuation parameter to compute successive equilibrium states.

We have first demonstrated that when the two vortices are far apart, the leading-order influence of one vortex on the other is well described by an external rotating strain field whose characteristics are provided by a point-vortex model. By considering a single vortex in that external strain field, we have shown that the elliptic deformation of each vortex near its center was very well reproduced even up to the large critical value of the strain rate for which the equilibrium states stop to exist. This result could be useful to determine the stability properties of the system with respect to the elliptical instability. Indeed, as mentioned in the Introduction, the inner strain rate provides an estimate for the maximum

FIG. 9. Minimum angular velocity Ω_o as a function of the strain rate γ_e for two corotating vortices (dashed line), a single vortex in a rotating strain field (dotted line), a single vortex in a higher order deformation field (solid line). Initial parabolic vorticity distribution in each case.
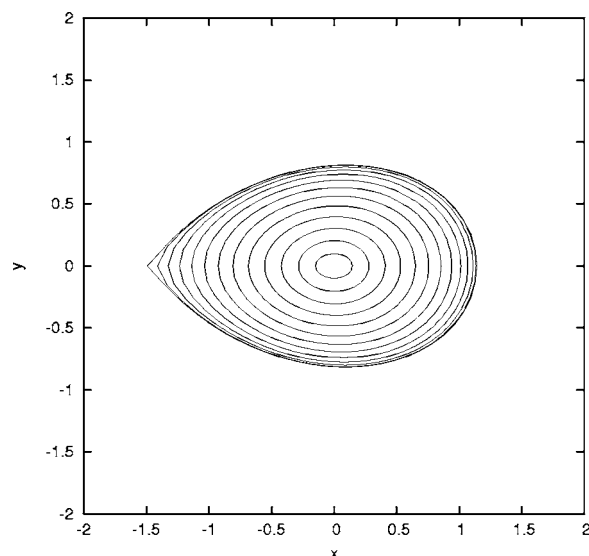
growth rate of this instability. If the two-vortex system and the vortex in the rotating strain field have the same inner strain rate, we can therefore conclude that they possess the same stability properties with respect to the elliptical instability. A theoretical model for the stability properties of a two-vortex system was recently constructed in Ref. 18 based on this assumption.

The paper has also been concerned with the determination of the critical parameters for which the equilibrium solutions stop to exist. These critical configurations have been identified as the situations where a stagnation point starts to penetrate into the vortex and a corner is forming at the outermost contour of vorticity. When the vorticity vanishes on the outer streamline, as for the parabolic profile, the critical configuration also corresponds to a change of stability in the sense that an eigenvalue of the Jacobian matrix of the nonlinear, parametrized system vanishes.

Based on the argument that the change of stability of the limiting configuration could correspond to the onset of merging, we have argued that this onset could be determined from the one-vortex model. In particular, we have shown that although the inner deformation was well predicted from the model of a vortex in a strain field, higher order terms in the deformation field were needed to describe correctly the asymmetric corner formation on the outer boundary of the vortex near the limit state. More precisely, we have shown that the minimal external deformation field is

$$\frac{1}{2}\hat{\gamma}_e(3x^2 + y^2) + \frac{1}{6}\sqrt{\frac{\pi}{\Gamma}}(2\hat{\gamma}_e)^{3/2}(3xy^2 - x^3) \tag{19}$$

with Γ the circulation of one vortex. Indeed, it has been shown that superimposing the above field (adding a term vx for the center of the vortex to remain a stagnation point) to the streamfunction generated by a single-vortex region, the topological changes of the outer vorticity contours, typical for the corotating vortices when they come closer together and ranging from the elliptical shape to the corner solution,

are accounted for. Furthermore, the critical strain rates $\hat{\gamma}_e / \omega_{max}$ have the same order of magnitude in both cases.

[1] R. R. Kerswell, "Elliptical instability," Annu. Rev. Fluid Mech. **34**, 83 (2002).

[2] H. K. Moffatt, S. Kida, and K. Ohkitani, "Stretched vortices -the sinews of turbulence; large-Reynolds-number asymptotics," J. Fluid Mech. **259**, 241 (1994).

[3] S. Le Dizès, "Non-axisymmetric vortices in two-dimensional flows," J. Fluid Mech. **406**, 175 (2000).

[4] S. Le Dizès and A. Verga, "Viscous interactions of two co-rotating vortices before merging," J. Fluid Mech. **467**, 389 (2002).

[5] D. Moore and P. Saffman, "Structure of a line vortex in an imposed strain," in *Aircraft Wake Turbulence and its Detection*, edited by J. Olsen, A. Goldberg, and N. Rogers (Plenum, New York, 1971).

[6] S. Kida, "Motion of an elliptic vortex in a uniform shear flow," J. Phys. Soc. Jpn. **50**, 3517 (1981).

[7] B. Legras and D. G. Dritschel, "Vortex stripping and the generation of high vorticity gradients in two-dimensional flows," Appl. Sci. Res. **51**, 445 (1993).

[8] B. Legras, D. G. Dritschel, and P. Caillou, "The erosion of a distributed two-dimensional vortex in a background straining flow," J. Fluid Mech. **441**, 369 (2001).

[9] P. G. Saffman and R. Szeto, "Equilibrium shapes of a pair of equal uniform vortices," Phys. Fluids **23**, 2339 (1980).

[10] D. G. Dritschel, "The stability and energetics of corotating uniform vortices," J. Fluid Mech. **157**, 95 (1985).

[11] M. V. Melander, N. J. Zabusky, and J. C. McWilliams, "Symmetric vortex merger in two dimensions: causes and conditions," J. Fluid Mech. **195**, 303 (1988).

[12] P. Meunier and T. Leweke, "Three-dimensional instability during vortex merging," Phys. Fluids **13**, 2747 (2001).

[13] C. Cerretelli and C. H. K. Williamson, "The physical mechanism of vortex merging," J. Fluid Mech. **475**, 41 (2003).

[14] P. Meunier, U. Ehrenstein, T. Leweke, and M. Rossi, "A merging criterion for two-dimensional co-rotating vortices," Phys. Fluids **14**, 2757 (2002).

[15] U. Ehrenstein and M. Rossi, "Equilibria of corotating nonuniform vortices," Phys. Fluids **11**, 3416 (1999).

[16] A. Mariotti, B. Legras, and D. Dritschel, "Vortex stripping and the erosion of coherent structures in two-dimensional flows," Phys. Fluids **6**, 3954 (1994).

[17] C. Cerretelli and C. H. K. Williamson, "A new family of uniform vortices related to vortex configurations before merging," J. Fluid Mech. **493**, 219 (2003).

[18] S. Le Dizès and F. Laporte, "Theoretical predictions for the elliptical instability in a two-vortex flow," J. Fluid Mech. **471**, 169 (2002).